fluids

MDPI

Article

A Reduced-Order Burgers-Type Vortex Model with Shear-Driven Gyroscopic Precession

Waleed Mouhali

Applied Mathematics Department, Lyrids, ECE, 10 rue Sextius-Michel, 75015 Paris, France; waleed.mouhali@ece.fr

Abstract

Slow lateral wandering and trochoidal-like motion are commonly observed in intense atmospheric vortices, yet most reduced-order vortex models assume a fixed axis or represent centre motion as purely advective. In this work, we propose a minimal reduced-order framework in which slow gyroscopic precession is introduced as an explicit degree of freedom superimposed on a rapidly rotating vortex core. The vortex is represented by a Burgers–Rott-type velocity field with time-dependent stretching rate and circulation, while the vortex centre undergoes a slow precessional motion governed by a time-dependent rate $\Omega_p(t)$. The evolution of the vortex parameters is coupled to environmental variability through simple relaxation laws driven by standard large-scale diagnostics, including convective available potential energy, vertical shear, and background vorticity. A tracker-only analysis of tropical cyclone best-track data is used to constrain the appropriate dynamical regime at the track scale, indicating that observed centre wandering typically occurs in a slow-precession limit $P = \Omega_p/\omega_c \ll 1$. Numerical demonstrations in cyclone-like configurations show that, despite the smallness of the precession number, cumulative lateral displacement and enhanced Lagrangian dispersion can develop over the vortex lifetime. The proposed framework is intended as a proof-of-concept reduced-order model that isolates the role of weak, environmentally forced precession in modulating vortex wandering and transport, and complements more detailed numerical and observational studies.

Keywords: gyroscopic precession; Burgers vortex; vortex dynamics; rotating flows; shear forcing; atmospheric vortices

1. Introduction

Intense atmospheric vortices such as tornadoes and tropical cyclones are among the most striking examples of coherent rotating structures in geophysical flows. Their dynamics result from a complex interplay between vorticity amplification, vortex stretching, environmental shear, and large-scale advection, spanning a wide range of spatial and temporal scales [1–3]. Despite their intrinsic complexity, simplified vortex representations have long played a central role in organizing observations, interpreting numerical simulations, and developing theoretical understanding.

1.1. Reduced Vortex Models in Atmospheric Flows

Analytical and semi-analytical vortex models provide a canonical language for describing rotating flows. Classical constructions such as Rankine vortices, Burgers vortices, and Burgers–Rott solutions capture, at various levels of approximation, the balance between rotation, strain, and diffusion in concentrated vortical structures [4,5]. In atmospheric

Check for updates

Academic Editor: Chaoqun Liu

Received: 11 February 2026
Revised: 2 March 2026
Accepted: 5 March 2026
Published: 10 March 2026

Copyright: © 2026 by the author. Licensee MDPI, Basel, Switzerland. This article is an open access article distributed under the terms and conditions of the Creative Commons Attribution (CC BY) license.

science, such models have been extensively used to interpret radar and numerical data of tornado-like vortices, to characterize core size and intensity, and to understand the role of axial stretching and viscous diffusion [6–10].

More elaborate reduced models have incorporated multiple cells, axial variation, or boundary-layer effects, and have been instrumental in clarifying the mechanisms leading to vortex intensification and maintenance [3,11]. However, most reduced-order approaches share a common assumption: at any instant, the vortex is treated as axisymmetric around a fixed or passively advected centre. Lateral motion of the vortex core is either prescribed externally or absorbed into background flow advection, rather than treated as an intrinsic degree of freedom. The focus of this work is therefore not on reproducing storm-specific dynamics, but on identifying a physically consistent reduced-order regime in which slow centre wandering can be represented explicitly and analyzed mechanistically.

1.2. Observed Wandering and Trochoidal Motion

In contrast with this modelling assumption, observations frequently show that the reported centre of intense atmospheric vortices exhibits slow lateral wandering or trochoidal-like motion superimposed on its mean translation. Such behaviour has been documented for tropical cyclones over time scales of one to several days and spatial excursions of tens of kilometres [12,13], and analogous wobbling behaviour has been reported in tornado-scale vortices in both radar observations and numerical simulations [14,15].

Several physical mechanisms have been proposed to explain this behaviour, including interactions with environmental shear, asymmetric convection, boundary-layer dynamics, and wave–mean-flow interactions such as vortex Rossby waves [16,17]. These studies provide valuable insight into the origin of asymmetries and unsteadiness in real storms. However, they typically rely on full three-dimensional numerical simulations or detailed diagnostic analyses, and do not translate directly into low-dimensional, analytically tractable models of vortex motion.

1.3. Precessing Vortices in Fluid Mechanics

Outside atmospheric science, slow precession of vortex cores is a well-established phenomenon in rotating flows. In swirling jets and combustors, a precessing vortex core (PVC) is a ubiquitous global mode that controls mixing, unsteadiness, and thermoacoustic coupling [18–21]. Similarly, rotating flows subjected to precessional forcing in laboratory containers exhibit coherent large-scale modes, including cyclonic vortices and inertial waves, whose dynamics are governed by gyroscopic balance and angular momentum constraints [22–24].

In these systems, precession arises naturally from the response of a rapidly rotating flow to an external torque, and can often be described in reduced form as a slow modulation superimposed on fast internal rotation. This fluid-mechanical perspective suggests that slow precession may be viewed as a generic response of rotating structures to asymmetric forcing, rather than as a phenomenon restricted to specific geometries or instabilities. In this context, precession should be understood as a reduced-order proxy for the cumulative effect of asymmetric forcing and environmental interaction, rather than as a claim about a single dominant physical instability. Figure 1 illustrates the type of slow centre wandering and trochoidal motion that motivates the reduced-order description proposed here.

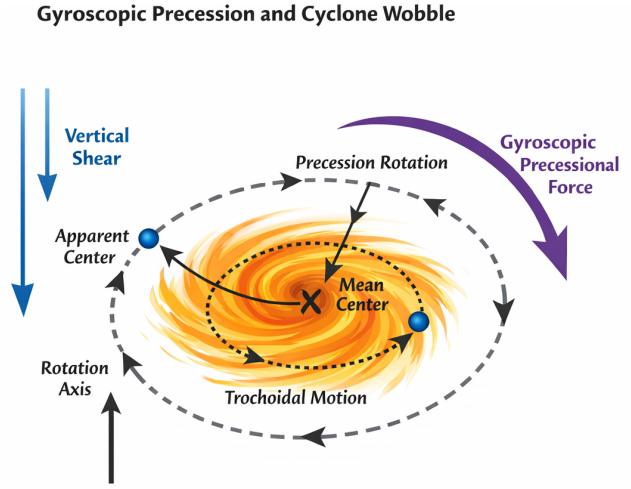


Figure 1. Schematic illustration of vortex centre wandering and trochoidal motion. The reported or apparent centre oscillates around a slowly varying guiding centre as a consequence of precessional motion induced by environmental shear. The dashed circle represents the precession path of radius R_p, while the intrinsic vortex rotation occurs on a much faster time scale.

1.4. Gap in the Literature

Despite these parallels, precession has remained largely absent from reduced-order models of atmospheric vortices. Existing analytical vortex models focus primarily on intensity, radial structure, and vertical coupling, while centre motion is either neglected or treated kinematically. Conversely, studies that address wandering or trochoidal motion typically do so within fully resolved simulations or observational diagnostics, without formulating a compact dynamical model that can be driven by large-scale environmental inputs.

As a result, there is currently no simple reduced-order framework that:

- Represents an atmospheric vortex as a rapidly rotating core with an explicit slow precession degree of freedom,
- Preserves an analytically tractable velocity field suitable for parameter studies and Lagrangian analysis,
- And allows direct forcing by standard environmental diagnostics such as convective available potential energy (CAPE), vertical shear, and background vorticity.

Consequently, there is currently no reduced-order framework that simultaneously (i) treats slow centre wandering as an explicit dynamical degree of freedom, (ii) preserves an analytically tractable vortex core, and (iii) is formulated in a regime where wandering is asymptotically weak ($P \ll 1$) but dynamically cumulative.

1.5. Approach and Contributions of the Present Work

The purpose of the present study is to bridge this gap by introducing a reduced-order vortex model in which slow gyroscopic precession is treated as an explicit, dynamically evolving degree of freedom. The vortex is represented by a Burgers–Rott-type velocity field whose stretching rate and circulation vary slowly in time, while the centre position undergoes a precessional motion characterized by a time-dependent rate $\Omega_p(t)$. The evolution of the vortex parameters is coupled to environmental variability through simple relaxation equations driven by CAPE, vertical shear, and large-scale vorticity. At tropical-cyclone scales, the effective diffusivity relevant to such reduced cores is dominated by turbulent processes, with values commonly inferred from axisymmetric hurricane simulations (e.g., [25]).

The modelling philosophy adopted here is deliberately minimal. The framework is barotropic and vertically reduced, and the environmental couplings are phenomenological rather than derived from first principles. The goal is not to reproduce storm-specific

dynamics, but to isolate and clarify the role of slow precession in modulating vortex wandering and Lagrangian transport in a setting that remains analytically transparent.

Using both synthetic forcing and reanalysis-driven inputs, we demonstrate that even when the precession number $P = \Omega_p/\omega_c$ is small, consistent with observational constraints, the cumulative effect of precession can produce substantial lateral displacement and enhanced tracer dispersion. In this sense, the model provides a compact fluid-mechanical bridge between environmental variability and vortex-scale transport, complementing more detailed numerical and observational approaches. Observational data are used here exclusively to constrain orders of magnitude and dynamical regimes, not to validate the model quantitatively. The present framework does not aim at reproducing specific inner-core instability mechanisms, but at providing a low-dimensional kinematic closure for slow centre wandering at the track scale.

While comprehensive dynamical models resolve the full complexity of tropical cyclone evolution, the multiplicity of interacting processes often obscures individual mechanisms. In particular, the contribution of weak environmental shear to slow trochoidal motion and long-time centroid drift typically emerges as a by-product of nonlinear multiscale interactions.

The objective of the present work is therefore not predictive realism, but mechanistic isolation. By introducing gyroscopic precession as an explicit slow degree of freedom superimposed on a rapidly rotating core, we construct a minimal analytical setting in which the ordering between intrinsic vortex rotation and externally forced drift becomes transparent. This allows the dimensionless precession number $P = \Omega_p/\omega_c$ to emerge as a structural control parameter.

The paper is organized as follows. Section 2 presents the reduced-order equations. Section 3 formulates the modelling problem and assumptions. Methods and results follow in Sections 4 and 5, respectively, and Section 6 discusses the implications and limitations of the proposed framework.

2. Model Equations

This section introduces the reduced-order equations governing the dynamics of a precessing atmospheric vortex. The formulation combines (i) an analytically tractable Burgers–Rott-type velocity field, (ii) an explicit kinematic description of vortex-centre precession, and (iii) a set of relaxation equations that couple the vortex parameters to slowly varying environmental forcing.

2.1. Instantaneous Vortex Velocity Field

At any instant, the horizontal velocity field associated with the vortex is assumed axisymmetric about its instantaneous centre position $\boldsymbol{x}_c(t) = (x_c(t), y_c(t))$. In a local polar coordinate system (r, θ) centred on $\boldsymbol{x}_c$, the velocity field is prescribed as a Burgers–Rott-type vortex,

$$u_r(r,t) = -a(t)\, r, \qquad u_\theta(r,t) = \frac{\Gamma(t)}{2\pi r}\left[1 - \exp\left(-\frac{r^2}{r_c^2}\right)\right], \tag{1}$$

where $a(t)$ is an effective stretching rate, $\Gamma(t)$ the circulation, and r_c a characteristic core radius. The exponential cutoff ensures regular behaviour near the origin and mimics viscous diffusion of vorticity.

It is important to clarify that the velocity field defined in Equation (1) is not intended to represent an exact time-dependent Navier–Stokes solution. In the classical Burgers vortex, the core radius r_c satisfies the viscous balance

$$r_c^2 = \frac{2\nu}{a}, \tag{2}$$

so that any time dependence of the stretching rate $a(t)$ would formally imply a corresponding evolution of the viscous core radius.

At atmospheric scale, however, the effective viscosity is dominated by turbulent processes. Using representative tropical cyclone parameters, with stretching rates of order $a \sim 10^{-5}\,\mathrm{s}^{-1}$ and turbulent effective viscosities $\nu_{\mathrm{eff}} \sim 10^{3}$–$10^{4}\,\mathrm{m}^{2}\,\mathrm{s}^{-1}$ (see, e.g., [25]), the Burgers balance yields

$$r_c \sim \sqrt{\frac{2\nu_{\mathrm{eff}}}{a}} \approx 15\text{–}45\ \mathrm{km}, \tag{3}$$

which is consistent with the observed inner-core radii of mature tropical cyclones.

This scaling indicates that the cyclone core radius is governed primarily by turbulent structural processes operating over synoptic time scales, rather than by instantaneous modulation of the stretching rate. For this reason, the present framework treats r_c as a structural parameter representative of the quasi-stationary inner-core scale, while intensity modulation and gyroscopic precession are introduced as slow reduced-order degrees of freedom. The model therefore operates in a physically consistent atmospheric regime, even though it does not enforce the instantaneous viscous Burgers balance.

This choice preserves the analytical simplicity of classical Burgers-type vortices while allowing the vortex intensity to evolve in time through the parameters $a(t)$ and $\Gamma(t)$. The velocity field is interpreted as a local, vertically reduced representation of the flow in a horizontal plane.

2.2. Centre Kinematics and Precession

The vortex centre is allowed to move in the horizontal plane under the combined effect of slow environmental translation and precessional wandering. As illustrated schematically in Figure 2, the vortex core is treated as a rapidly rotating column responding to environmental shear through slow gyroscopic precession. Its position is decomposed as

$$\boldsymbol{x}_c(t) = \boldsymbol{x}_s(t) + \boldsymbol{x}_p(t), \tag{4}$$

where $\boldsymbol{x}_s(t)$ denotes the guiding-centre trajectory associated with large-scale advection, and $\boldsymbol{x}_p(t)$ a residual displacement due to precession.

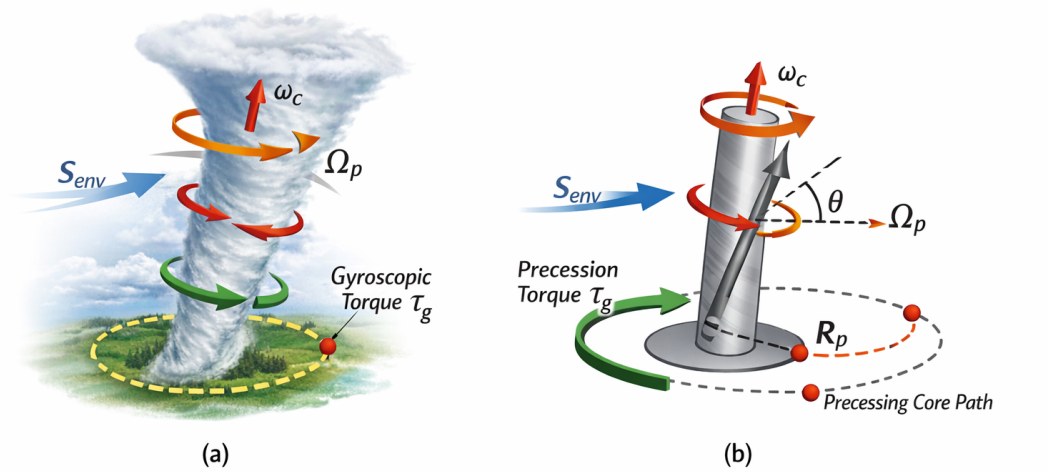


Figure 2. Conceptual representation of a rotating atmospheric vortex subjected to environmental shear. The rapidly rotating core (angular velocity ω_c) responds to an external torque induced by large-scale shear S_{env} through a slow gyroscopic precession at rate $\Omega_p \ll \omega_c$. Panel (**a**) illustrates the atmospheric interpretation, while panel (**b**) shows the reduced mechanical analogue used to motivate the precession kinematics.

The precessional motion is modelled kinematically as a circular orbit of fixed radius R_p,

$$\boldsymbol{x}_p(t) = R_p \begin{pmatrix} \cos\phi(t) \\ \sin\phi(t) \end{pmatrix}, \qquad \frac{\mathrm{d}\phi}{\mathrm{d}t} = \Omega_p(t), \tag{5}$$

where $\phi(t)$ is the precession phase and $\Omega_p(t)$ the instantaneous precession rate.

This formulation explicitly separates the fast internal rotation of the vortex from the slow evolution of its centre position. In particular, the assumption $\Omega_p \ll \omega_c$ ensures that precession acts as a weak, low-frequency modulation rather than as a dominant dynamical instability.

2.3. Environmental Forcing and Relaxation Dynamics

The evolution of the vortex parameters $a(t)$, $\Gamma(t)$, and $\Omega_p(t)$ is governed by first-order relaxation toward target values prescribed by the large-scale environment:

$$\frac{\mathrm{d}a}{\mathrm{d}t} = \frac{a^\star(t) - a(t)}{\tau_a}, \qquad \frac{\mathrm{d}\Gamma}{\mathrm{d}t} = \frac{\Gamma^\star(t) - \Gamma(t)}{\tau_\Gamma}, \qquad \frac{\mathrm{d}\Omega_p}{\mathrm{d}t} = \frac{\Omega_p^\star(t) - \Omega_p(t)}{\tau_\Omega}. \tag{6}$$

Here τ_a, τ_Γ, and τ_Ω are characteristic adjustment time scales that are assumed to be long compared with the internal rotation period but short compared with the time scale of environmental variability.

The target values $(a^\star, \Gamma^\star, \Omega_p^\star)$ are constructed from standard environmental diagnostics:

$$a^\star(t) = \frac{\sqrt{2\,\mathrm{CAPE}(t)}}{L_z}, \tag{7}$$

$$\Gamma^\star(t) = \gamma\,\zeta_{\mathrm{env}}(t)\,\pi r_c^2, \tag{8}$$

$$\Omega_p^\star(t) = \alpha\,|S(t)|, \tag{9}$$

where $\mathrm{CAPE}(t)$ is the convective available potential energy, $S(t)$ the bulk vertical shear magnitude, and $\zeta_{\mathrm{env}}(t)$ the environmental vorticity. The coefficients α and γ represent effective coupling efficiencies, while L_z is a representative convective depth.

Interpretation and physical scaling. CAPE provides a characteristic vertical velocity scale through $w \sim \sqrt{2\,\mathrm{CAPE}}$. A representative stretching rate is then estimated as a vertical gradient $a \sim \partial_z w \sim w/L_z$, which yields Equation (7). This closure is used here as an order-of-magnitude reduced forcing rather than as a first-principles derivation.

Equation (8) is intended as a minimal ingestion/aggregation closure: environmental vorticity ζ_{env} contributes to the core circulation over an effective area πr_c^2. The coefficient γ summarizes unresolved efficiency factors (e.g., asymmetric convection, mixing, and boundary-layer inflow) and is therefore treated as phenomenological in the present proof-of-concept framework.

This closure reflects the modelling philosophy adopted here: commonly used meteorological diagnostics are treated as time-dependent forcings that continuously modulate vortex intensity and precession, rather than as static indices of storm potential.

2.4. Non-Dimensional Form and Control Parameters

To clarify the governing parameter regime, we introduce a characteristic angular velocity

$$\omega_c = \frac{\Gamma_0}{2\pi r_c^2}, \tag{10}$$

where Γ_0 is a reference circulation, and define the non-dimensional precession number

$$P(t) = \frac{\Omega_p(t)}{\omega_c}. \tag{11}$$

The reduced dynamics are thus controlled by a small set of dimensionless parameters: the precession number P, ratios of relaxation time scales to the rotation period $(\tau_i \omega_c)^{-1}$, and the relative amplitudes of the environmental forcings. The present study focuses on the asymptotic regime $P \ll 1$, consistent with both the modelling assumptions and the tracker-derived constraints presented in Section 5.

2.5. Particle Advection and Diagnostics

Lagrangian transport is probed by advecting passive tracers with the instantaneous velocity field,

$$\frac{\mathrm{d}\boldsymbol{x}}{\mathrm{d}t} = \boldsymbol{u}\big(\boldsymbol{x} - \boldsymbol{x}_c(t), t\big), \tag{12}$$

where $\boldsymbol{u}$ is defined by Equation (1) in the vortex-centred frame. Tracer trajectories are used to visualize near-core mixing, quantify lateral dispersion, and compare precessing and non-precessing configurations under identical forcing histories.

Together, Equations (1)–(12) define a closed, low-dimensional system that couples vortex intensity, precession, and environmental forcing in an analytically transparent manner.

3. Problem Formulation

3.1. Physical Question and Modelling Objective

Large-scale atmospheric vortices such as tornadoes and tropical cyclones are characterized by a fast internal rotation combined with slower variations of their structure and position. In observations and simulations, the reported vortex centre often exhibits low-frequency lateral wandering or trochoidal-like motion superimposed on its mean translation. While such behaviour is routinely documented, it is rarely represented explicitly in reduced-order vortex models, which typically prescribe a fixed axis or treat centre motion as purely advective.

The central question addressed in this work is therefore the following:

> *How can slow lateral wandering of an intense atmospheric vortex be represented within a minimal, analytically tractable reduced-order model, while preserving a clear separation between fast internal rotation and slow environmental modulation?*

Our objective is not to reproduce the full three-dimensional structure of real storms, nor to identify the microscopic origin of asymmetric dynamics. Instead, we seek a compact formulation that isolates the kinematic and dynamical consequences of a *slow gyroscopic degree of freedom* associated with vortex precession, and that can be forced directly by large-scale environmental diagnostics.

3.2. Reduced-Order Viewpoint and Time-Scale Separation

We adopt a reduced-order modelling perspective in which the vortex is treated as a coherent rotating structure characterized by a small set of internal parameters and embedded in a slowly varying environment. The key assumption is a separation of time scales between:

- The fast internal rotation of the vortex, with characteristic angular velocity ω_c,
- Intermediate adjustment processes associated with stretching and circulation,
- Slow lateral wandering or precession of the vortex axis, with characteristic rate Ω_p,
- And even slower environmental variability.

This ordering can be summarized as

$$\Omega_p \ll \omega_c,$$

or, in non-dimensional form, by a small precession number

$$P = \frac{\Omega_p}{\omega_c} \ll 1.$$

The tracker-only results presented later show that observed tropical cyclones indeed operate in such a regime, with P_{obs} typically of order 10^{-2}. This empirical constraint motivates the asymptotic structure of the reduced model and legitimizes treating precession as a slow, weakly coupled degree of freedom.

3.3. Vortex Representation and Modelling Assumptions

Within this framework, the vortex is idealized as a vertically oriented, axisymmetric rotating core whose instantaneous horizontal velocity field remains close to that of a Burgers–Rott-type vortex. This choice is motivated by the analytical tractability of Burgers-type solutions and their long-standing use as canonical models of stretched viscous vortices in both turbulence and atmospheric flows [4,5,26].

The model makes the following explicit assumptions:

1. **Barotropic, vertically reduced dynamics.** The flow is represented in a horizontal plane, with vertical structure entering only through an effective stretching rate. Stratification, moist processes, and explicit baroclinic vorticity generation are neglected.
2. **Axisymmetric internal structure.** At any instant, the internal velocity field is assumed axisymmetric about the vortex centre, even though the centre itself may move.
3. **Explicit centre dynamics.** The vortex centre is allowed to undergo a slow precessional motion, treated as an independent kinematic degree of freedom.
4. **Environmental forcing through low-order diagnostics.** Large-scale quantities such as CAPE, vertical shear, and background vorticity act as time-dependent forcings on the reduced variables via relaxation-type closures.

These assumptions deliberately exclude detailed inner-core asymmetries, boundary-layer processes, and fully three-dimensional instabilities. The goal is not completeness, but clarity: to isolate how slow precession interacts with vortex intensity and transport in the simplest possible setting.

3.4. Gyroscopic Precession as a Modelling Principle

The introduction of precession is inspired by analogies with rotating flows subjected to external torques, where a rapidly spinning structure responds through a slow gyroscopic motion of its axis. Such behaviour is well documented in precessing laboratory flows and rotating containers [22–24], as well as in swirling jets and combustors exhibiting precessing vortex cores.

In the present context, precession should not be interpreted as a literal rigid-body motion. Rather, it provides a low-dimensional proxy for the cumulative effect of asymmetric forcing, shear, and environmental interactions on the lateral position of the vortex core. By introducing an explicit precession rate $\Omega_p(t)$, the model allows this slow wandering to be represented transparently and to be coupled directly to measurable environmental inputs.

3.5. Scope of the Present Study

Consistent with the above formulation, the present work focuses on:

- Defining a reduced-order vortex model with an explicit precession degree of freedom,
- Demonstrating that slow precession can produce dynamically significant lateral wandering even when $P \ll 1$,
- And establishing order-of-magnitude consistency between the model regime and observed cyclone tracks.

Quantitative calibration, parameter optimization, and storm-specific prediction are intentionally left outside the scope of this paper. These aspects require either high-resolution simulations or richer observational datasets and form the natural basis for subsequent work building on the formulation introduced here.

4. Methods

This section describes the data sources and processing steps used to extract track-scale wandering and to estimate an observed precession rate from cyclone best-track data. The methodology is deliberately kinematic and low-order, in order to remain consistent with the reduced-order modelling approach adopted throughout the paper. All the details can be found in Appendix A.

4.1. Best-Track Data

Storm-centre positions are taken from standard best-track datasets, which provide six-hourly estimates of cyclone location, intensity, and maximum sustained wind speed. For Atlantic hurricanes, we use the HURDAT2 database maintained by the National Hurricane Center, while IBTrACS is used as a complementary source to ensure consistency across basins. The analyzed cases (Hugo, Hyacinthe, Katrina) were selected based on data completeness and sustained intensity over multi-day periods.

Best-track positions represent an operational estimate of the large-scale storm centre and are not intended to resolve inner-core structure or mesoscale asymmetries. In the present work, they are treated as a coarse-grained representation of vortex translation suitable for analyzing track-scale wandering on time scales of order one day or longer.

4.2. Guiding-Centre Extraction

To separate the slow translation of the storm from residual wandering, the observed centre trajectory $\mathbf{r}_{\mathrm{obs}}(t)$ is decomposed as

$$\mathbf{r}_{\mathrm{obs}}(t) = \mathbf{r}_s(t) + \mathbf{r}'(t),$$

where $\mathbf{r}_s(t)$ is a guiding-centre trajectory and $\mathbf{r}'(t)$ a residual displacement.

The guiding centre is obtained by applying a temporal smoothing filter to each horizontal coordinate independently. We use a low-pass moving-average filter with a window of 24–36 h, chosen to remove synoptic-scale translation while retaining variability on time scales longer than the dominant internal rotation of the vortex. Tests with window sizes in this range yield qualitatively similar residuals, indicating limited sensitivity to the precise choice of filter length.

The residual displacement $\mathbf{r}'(t)$ represents low-frequency lateral wandering of the reported storm centre relative to its guiding trajectory.

4.3. Phase and Angular-Rate Estimation

The residual trajectory $\mathbf{r}'(t)$ is expressed in polar coordinates,

$$\mathbf{r}'(t) = A(t)[\cos\phi(t), \sin\phi(t)],$$

where $A(t) = |\mathbf{r}'(t)|$ is the instantaneous wobble amplitude and $\phi(t)$ the phase angle. The phase is unwrapped in time, and the instantaneous angular rate is estimated by finite differencing,

$$\Omega_{\text{obs}}(t) = \frac{\mathrm{d}\phi(t)}{\mathrm{d}t}.$$

When the residual amplitude $A(t)$ becomes small, the phase estimate becomes ill-conditioned and can produce spurious large values of Ω_{obs}. Such excursions are treated as numerical artefacts of the phase definition rather than as physically meaningful events. Accordingly, when reporting statistical values of Ω_{obs} and P_{obs}, we apply an amplitude-based quality control: time instants for which $A(t) < A_{\text{th}}$ are excluded from the statistical summaries, where A_{th} is chosen as a small fraction of the typical wobble amplitude (e.g., $A_{\text{th}} = 0.1\,\text{median}(A)$). This filtering prevents phase noise when $A(t) \to 0$ from contaminating the inferred precession statistics.

4.4. Definition of the Observed Precession Number

To compare the extracted angular rate with the intrinsic rotation of the vortex, we define a characteristic inner-core angular velocity

$$\omega_c = \frac{V_{\text{max}}}{r_c},$$

where V_{max} is the maximum sustained wind speed reported in the best-track data and r_c a representative core radius. In the absence of a consistently reported radius of maximum wind, r_c is chosen within a physically reasonable range for tropical cyclones (typically 20–50 km), and sensitivity to this choice is assessed by repeating the calculation over this interval.

The non-dimensional observed precession number is then defined as

$$P_{\text{obs}}(t) = \frac{\Omega_{\text{obs}}(t)}{\omega_c}.$$

This quantity measures the ratio between the time scale of track-scale wandering and that of the internal vortex rotation. Throughout this work, P_{obs} is interpreted as an order-of-magnitude indicator of dynamical regime rather than as a precise storm-specific parameter.

4.5. Minimal Kinematic Reconstruction

To illustrate the scale and geometry of the extracted wandering, we construct a minimal kinematic reconstruction of the observed track. The reconstructed centre position is defined as

$$\mathbf{r}_{\text{mod}}(t) = \mathbf{r}_s(t) + R_p\left[\cos\left(\Omega_p t\right), \sin\left(\Omega_p t\right)\right],$$

where R_p is taken as the median wobble amplitude and Ω_p as a representative mean value of Ω_{obs} over the analysis window.

This reconstruction is not a dynamical fit but a geometrical illustration showing that a single precession mode superimposed on guiding-centre motion captures the dominant amplitude and time scale of the observed residual displacement. It is used solely to visualize the relevance of a precession-based description and not as a validation of a physical precession mechanism.

4.6. Minimal Lagrangian Transport Diagnostic

To provide a quantitative yet lightweight assessment of the effect of slow core precession, we compute a Lagrangian transport diagnostic based on passive tracer advection in the reduced horizontal velocity field. Tracer positions $\boldsymbol{x}_i(t)$ satisfy

$$\frac{d\boldsymbol{x}_i}{dt} = \boldsymbol{u}_\perp(\boldsymbol{x}_i(t), t), \tag{13}$$

where $\boldsymbol{u}_\perp$ is given by Equations (1)–(5). We compare two configurations with identical vortex parameters (a, Γ, r_c): a reference case with a fixed core ($\Omega_p = 0$) and a precessing-core case with prescribed circular motion at constant precession rate Ω_p.

A total of $N = 600$ passive tracers are initially seeded within $r \leq 2r_c$ around the guiding centre and integrated over a multi-day window using a second-order Runge–Kutta scheme. We report two complementary transport measures: (i) the mean-squared displacement

$$\mathrm{MSD}(t) = \frac{1}{N}\sum_{i=1}^{N} |\boldsymbol{x}_i(t) - \boldsymbol{x}_i(0)|^2,$$

and (ii) the area $A(t)$ of the convex hull enclosing all tracer positions, which quantifies the effective horizontal footprint of the cloud. These metrics are evaluated identically for both cases to isolate the impact of slow precession on cumulative dispersion.

All numerical simulations were performed in Python (Python 3.10), using NumPy for computation and Matplotlib for visualization. Lagrangian trajectories were integrated using a second-order Runge–Kutta (RK2) time-stepping scheme.

5. Results

This section presents numerical and data-driven results illustrating the behaviour of the reduced precessing-vortex framework. We first use best-track cyclone data to extract an order-of-magnitude estimate of track-scale precession, which constrains the dynamical regime relevant to the model. We then show that a minimal kinematic reconstruction based on guiding-centre motion plus slow precession reproduces the observed scale and frequency of centre wandering. Throughout this section, the emphasis is on regime consistency and scaling rather than storm-specific validation.

5.1. Tracker-Only Reconstruction of Centre Wandering

We analyse best-track centre positions for three intense tropical cyclones (Hugo, Hyacinthe, and Katrina) using a purely kinematic decomposition. The observed storm-centre trajectory $\mathbf{r}_{\mathrm{obs}}(t)$ is separated into a slowly varying guiding-centre component $\mathbf{r}_s(t)$ obtained by temporal smoothing, and a residual motion $\mathbf{r}'(t) = \mathbf{r}_{\mathrm{obs}}(t) - \mathbf{r}_s(t)$ that captures low-frequency wandering. This decomposition is designed to isolate track-scale "wobble" rather than inner-core or mesoscale asymmetries.

Figure 3 shows the result for Hurricane Hugo. The observed track (blue) departs systematically from the smoothed guiding trajectory (orange), indicating a persistent residual motion over time scales of order days. A minimal kinematic reconstruction is overlaid (green), in which the residual is modelled as a circular precession of constant radius and angular rate around the guiding centre. Despite its simplicity, this reconstruction captures the amplitude and characteristic period of the observed wandering.

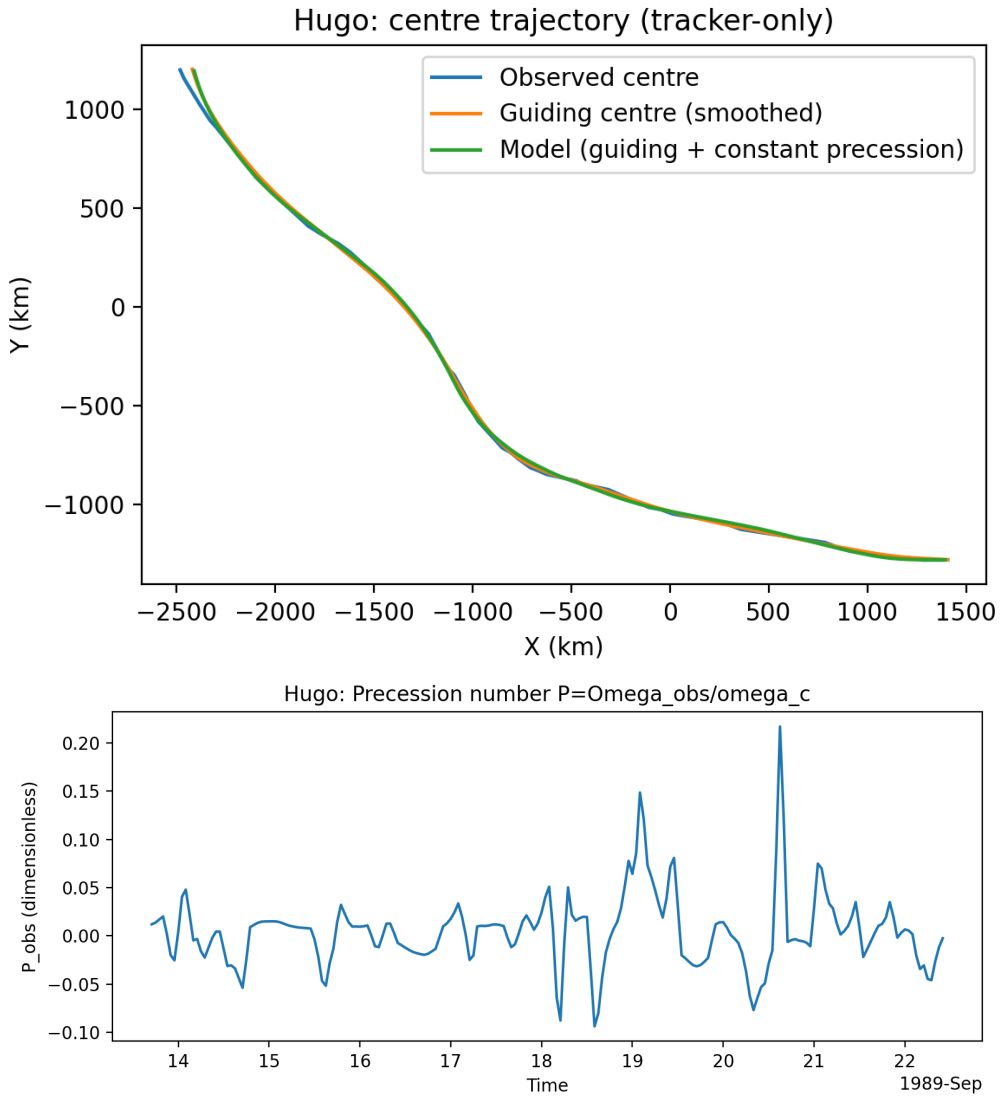


Figure 3. Tracker-only analysis for Hurricane Hugo. (**top**) Observed storm centre trajectory (blue), smoothed guiding centre (orange), and minimal kinematic reconstruction obtained by superimposing a constant precession on the guiding track (green). (**bottom**) Time series of the inferred non-dimensional precession number $P_{\mathrm{obs}} = \Omega_{\mathrm{obs}}/\omega_c$. Values are typically $\mathcal{O}(10^{-2})$, with intermittent spikes associated with low residual amplitude and phase ill-conditioning. The guiding centre is obtained by temporal smoothing over a multi-day window, isolating the low-frequency component of centre motion.

Equivalent decompositions for Hurricanes Hyacinthe and Katrina are shown in Figures 4 and 5, respectively. In all three cases, the centre motion exhibits a combination of smooth large-scale translation and superimposed low-frequency lateral displacement. While the precise geometry of the residual varies between storms, the existence of a slowly varying wandering mode is robust across cases.

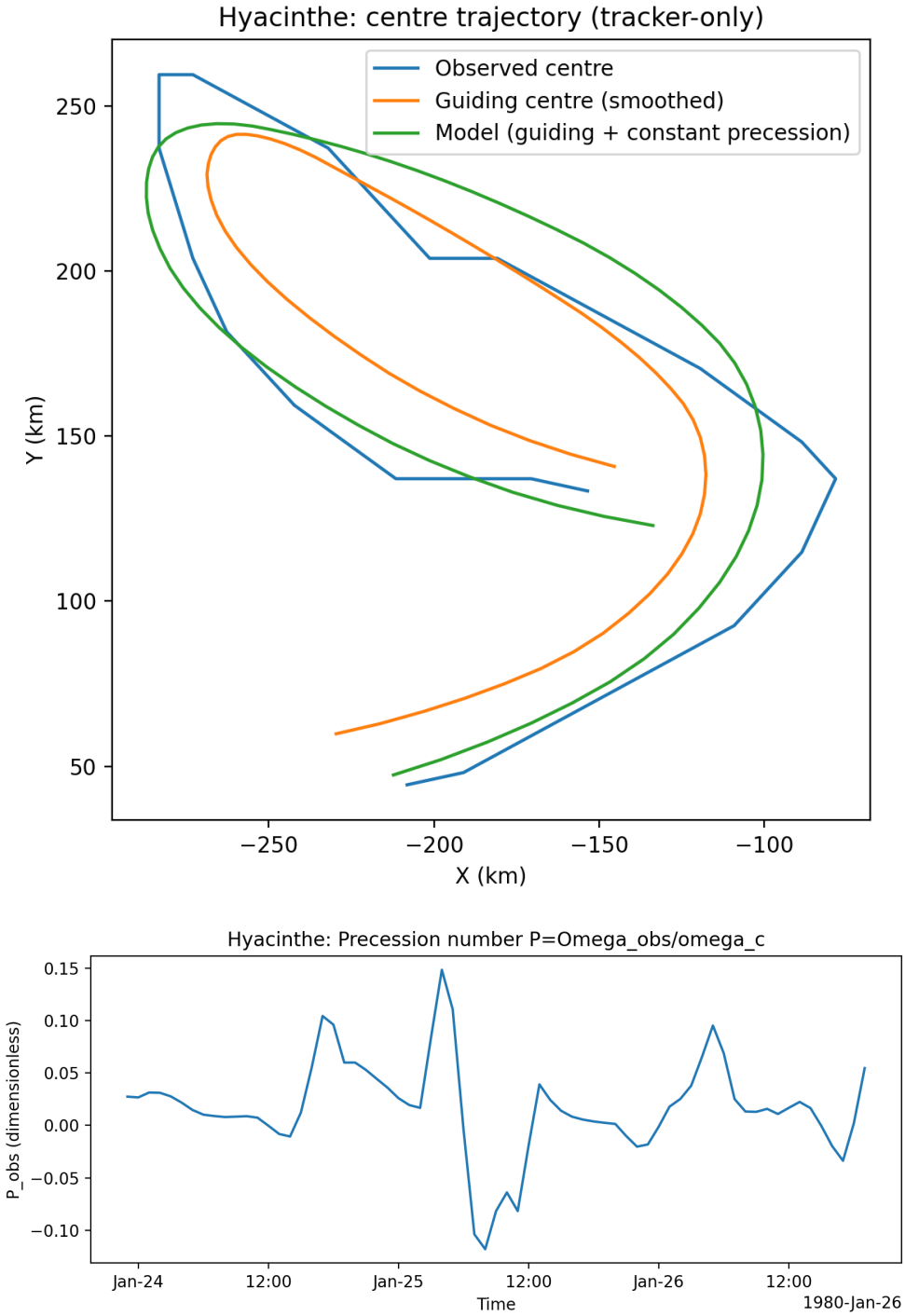


Figure 4. Same as Figure 3 for Tropical Cyclone Hyacinthe. The extracted centre wandering occurs on multi-day time scales and yields a precession number $|P_{\mathrm{obs}}| \sim 10^{-2}$, slightly larger on average than in Hurricane Hugo due to a smaller inferred internal rotation rate ω_c. The guiding centre is obtained by temporal smoothing over a multi-day window, isolating the low-frequency component of centre motion.

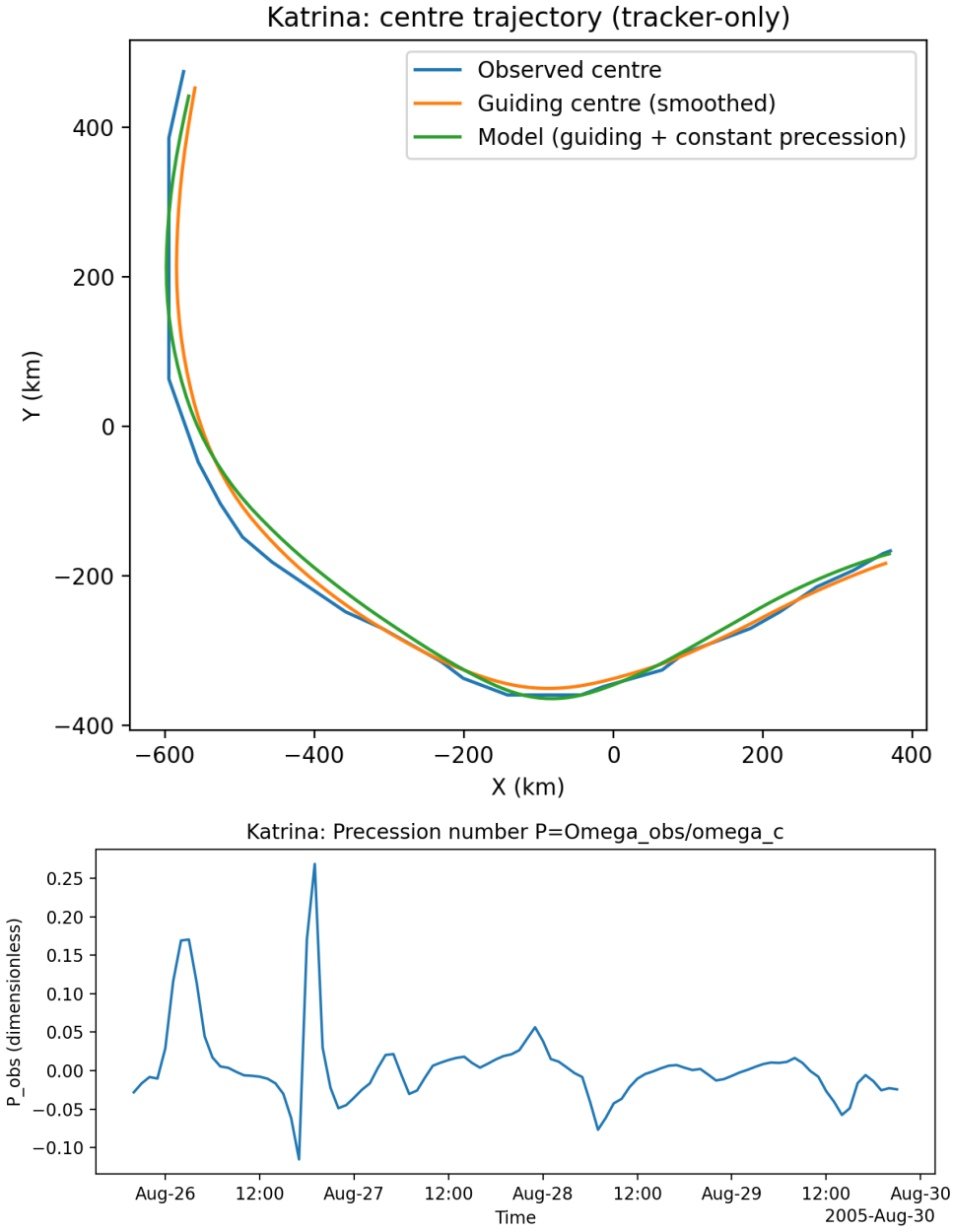


Figure 5. Same as Figure 3 for Hurricane Katrina. The tracker-derived precession number remains small ($P_{\mathrm{obs}} \ll 1$), consistent with slow eye wandering and trochoidal-like motion superimposed on the large-scale storm track. The guiding centre is obtained by temporal smoothing over a multi-day window, isolating the low-frequency component of centre motion.

5.2. Estimated Precession Number and Dynamical Regime

From the residual motion $\mathbf{r}'(t)$, we extract an instantaneous phase $\phi_{\mathrm{obs}}(t)$ and angular rate $\Omega_{\mathrm{obs}}(t) = \mathrm{d}\phi_{\mathrm{obs}}/\mathrm{d}t$ using finite differences on the smoothed phase signal. To assess the relevance of this wandering for vortex dynamics, we normalize Ω_{obs} by a characteristic inner-core angular velocity

$$\omega_c = \frac{V_{\max}}{r_c},$$

where $V_{\max}$ is the reported maximum wind speed and r_c a representative core radius. This defines an observed precession number

$$P_{\mathrm{obs}}(t) = \frac{\Omega_{\mathrm{obs}}(t)}{\omega_c}.$$

The time evolution of $P_{\text{obs}}(t)$ for Hurricane Hugo is shown in Figure 3. The signal fluctuates around zero with typical magnitudes $|P_{\text{obs}}| \sim 10^{-2}$ and intermittent spikes. These spikes coincide with times when the residual amplitude is small and the phase becomes poorly conditioned; they are therefore not interpreted as physically meaningful extremes. The relevant metric is the typical or median magnitude of P_{obs}, which remains well below unity.

Figures 4 and 5 show the corresponding results for Hyacinthe and Katrina.

Across all three storms, the inferred precession number typically remains $\mathcal{O}(10^{-2})$ and therefore well below unity, indicating a clear separation between fast internal rotation and slow track-scale wandering. This ordering directly supports the asymptotic regime assumed in the reduced precessing-vortex model, in which gyroscopic precession acts as a slow degree of freedom superimposed on rapid swirl.

Figure 6 extends the single-parameter demonstration by exploring one order of magnitude variation in the precession number ($P = 10^{-3}, 10^{-2}, 10^{-1}$) and two representative precession radii.

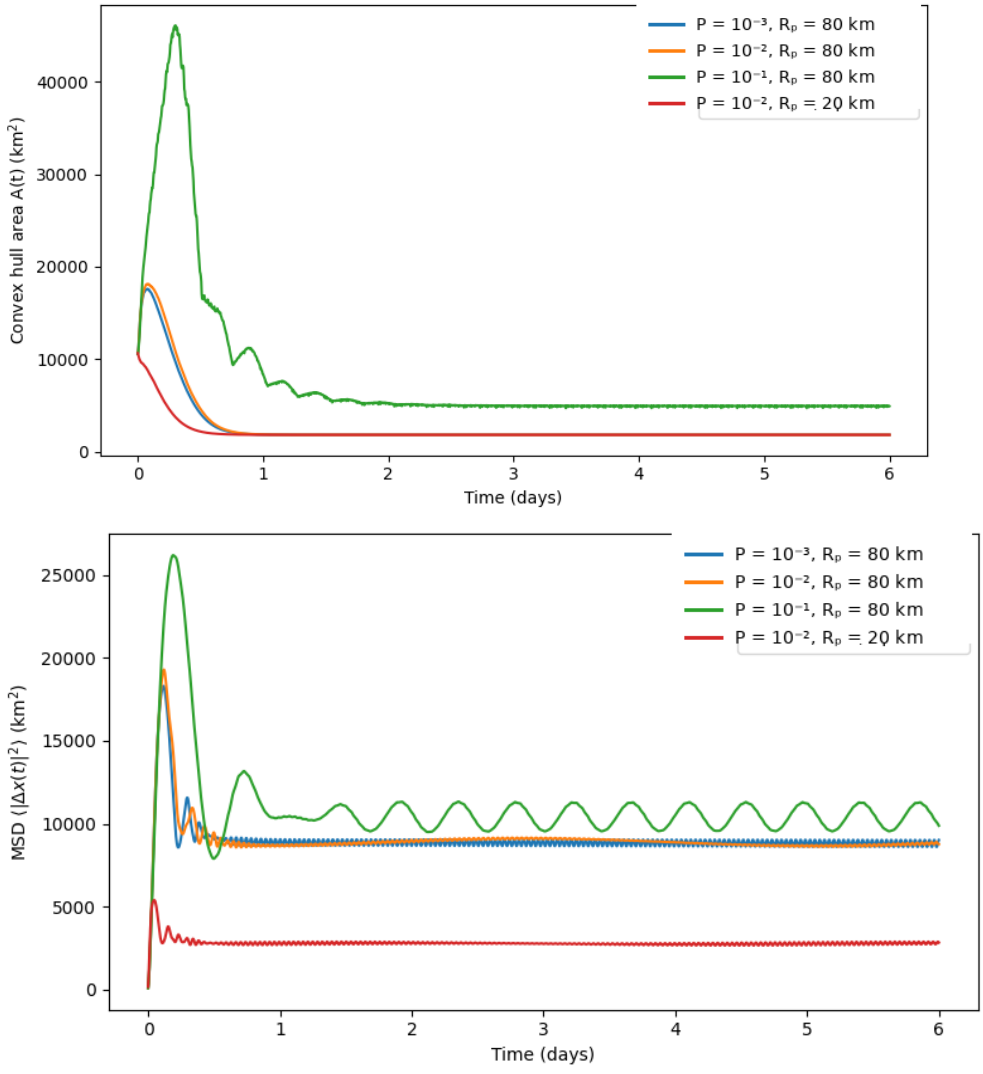


Figure 6. Lagrangian diagnostics in a cyclone-like configuration. (**Top**) mean-square displacement (MSD) for $P = 10^{-3}, 10^{-2}, 10^{-1}$ and two choices of precession radius ($R_p = 80$ km and $R_p = 20$ km). (**Bottom**) convex-hull area under the same parameter variations. The dispersion enhancement persists across one order of magnitude in P and scales naturally with R_p, including the control case $R_p = 20$ km representative of observed wobble amplitudes.

Several robust features emerge. First, the enhancement of long-time dispersion is present for all non-zero values of P, indicating that precession acts as a cumulative transport mechanism even in the strongly asymptotic regime $P \ll 1$. As P increases, the onset of divergence between precessing and non-precessing configurations occurs earlier in time, consistent with the shorter precession period.

Second, the magnitude of the dispersion scales naturally with the geometric amplitude R_p. When R_p is reduced to values comparable to the observed wobble amplitude ($R_p \simeq 20$ km), the enhancement remains clearly detectable but with reduced absolute magnitude. This confirms that the transport effect is not an artefact of an exaggerated precession radius, but a structural consequence of slow lateral core motion.

Taken together, these results demonstrate that weak gyroscopic precession produces a robust, parameter-insensitive amplification of multi-day Lagrangian dispersion in cyclone-like configurations.

5.3. A Minimal Quantitative Metric: Precession-Enhanced Lagrangian Dispersion

To provide a quantitative, journal-standard result beyond qualitative track reconstructions, we compute a Lagrangian transport diagnostic from passive-tracer advection in the horizontally reduced model. We integrate

$$\dot{\boldsymbol{x}}_i(t) = \boldsymbol{u}_\perp(\boldsymbol{x}_i(t), t), \qquad i = 1, \ldots, N,$$

for $N = 600$ tracers initially seeded within $r \leq 2r_c$ around the vortex centre. We compare a reference case with a fixed core ($\Omega_p = 0$) to a weak-precession case with prescribed circular core motion (1)–(5) at precession number $P = \Omega_p/\omega_c = 10^{-2}$, precession radius $R_p = 80$ km, and period $T_p = 2\pi/\Omega_p \simeq 4.4$ days. The Burgers-type parameters are chosen to represent a cyclone-like inner core with $r_c = 30$ km and characteristic swirl $V_{\max} \simeq 50\ \mathrm{m\,s^{-1}}$ (setting $\omega_c = V_{\max}/r_c$). The strain rate is fixed to $a = 3 \times 10^{-5}\ \mathrm{s^{-1}}$ (order 10 h time scale), and Γ is selected so that $u_\theta(r_c) \approx V_{\max}$. The early-time peak in MSD for the non-precessing case reflects rapid ejection of tracers initially located in the high-strain region r > rc; after this transient, both cases settle into a slower diffusive regime.

We report two complementary metrics: (i) the mean-squared displacement (MSD) $\langle |\Delta \boldsymbol{x}(t)|^2 \rangle = \frac{1}{N} \sum_{i=1}^{N} |\boldsymbol{x}_i(t) - \boldsymbol{x}_i(0)|^2$, and (ii) the convex-hull area $A(t)$ of the tracer cloud (a compact measure of the occupied horizontal footprint). Figure 6 shows that, despite $P \ll 1$, precession yields a clear, order-unity increase in long-time MSD relative to the non-precessing vortex, demonstrating that weak core wandering acts as an efficient Lagrangian disperser over multi-day time scales.

5.4. Interpretation as a Regime Constraint Rather than a Validation

It is important to emphasize that the tracker-only analysis is not intended as a quantitative validation of the reduced model. Best-track positions provide a coarse representation of storm motion and do not resolve inner-core structure, asymmetric eyewall dynamics, or boundary-layer processes. Accordingly, the extracted Ω_{obs} and P_{obs} should be interpreted as *order-of-magnitude constraints* on low-frequency centre wandering, not as precise measurements of a physical precession mechanism.

Within this interpretation, the results serve a specific purpose: they demonstrate that observed tropical-cyclone motion occupies a regime in which slow precession ($P \ll 1$) is dynamically plausible and potentially relevant over multi-day time scales. This justifies the modelling choice adopted in the present work, where precession is treated as a weak but cumulative kinematic effect rather than as a dominant instability.

In the following sections, this regime constraint motivates the numerical experiments performed with the reduced Burgers-type vortex model, where environmental forcing

modulates the stretching, circulation, and precession rate in a controlled and analytically tractable setting.

5.5. Sensitivity to the Core Radius r_c

Because the non-dimensional precession number is defined as

$$P = \frac{\Omega_p}{\omega_c}, \qquad \omega_c \simeq \frac{V_{\max}}{r_c}, \tag{14}$$

it depends linearly on $1/r_c$ for fixed $V_{\max}$ and Ω_p. The inferred dynamical regime is therefore sensitive to the assumed inner-core radius.

To quantify this dependence, we recompute $P_{\text{model}}(t)$ for

$$r_c \in \{20, 30, 40, 50\} \text{ km},$$

covering the typical range of tropical-cyclone inner-core radii reported in the literature.

Figure 7 reports the resulting time series for the three analyzed storms: (*top*) Hurricane Hugo, (*middle*) Cyclone Hyacinthe, and (*bottom*) Hurricane Katrina. In each case, decreasing r_c increases P_{model} as expected from the scaling $P \propto 1/r_c$.

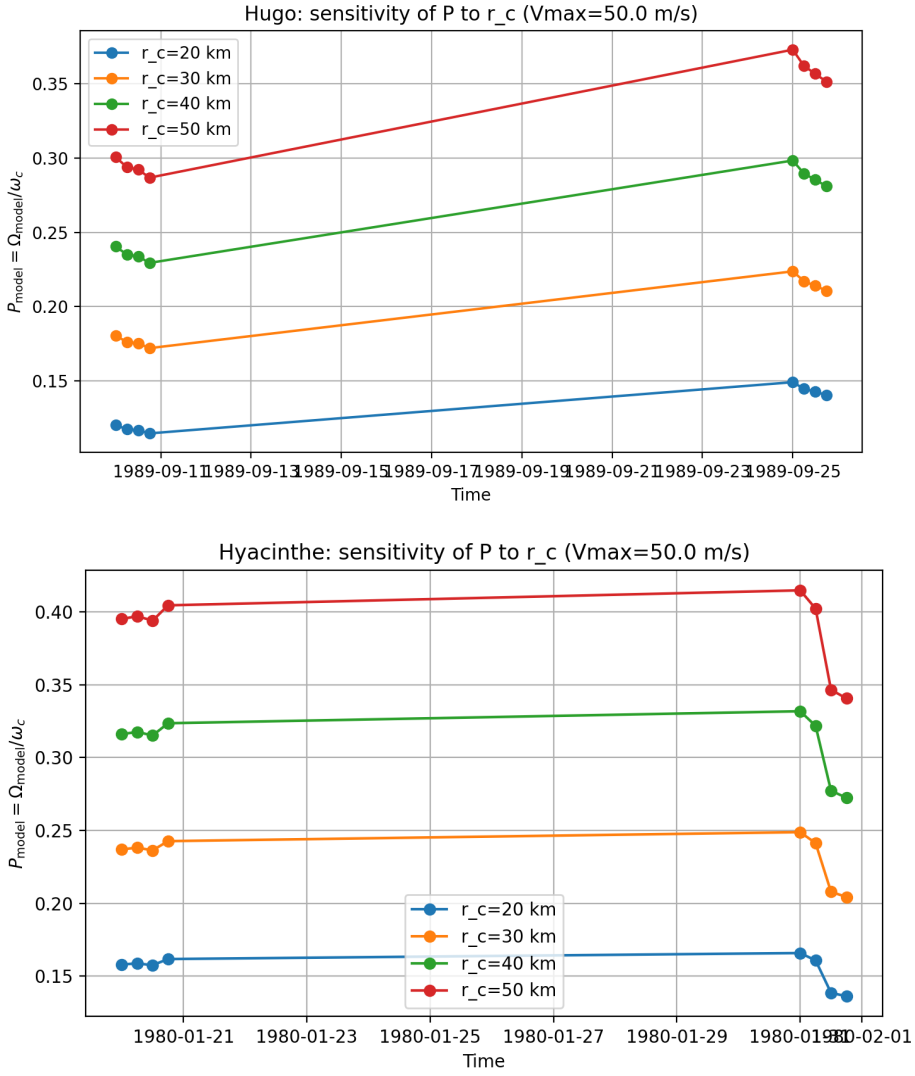


Figure 7. *Cont.*

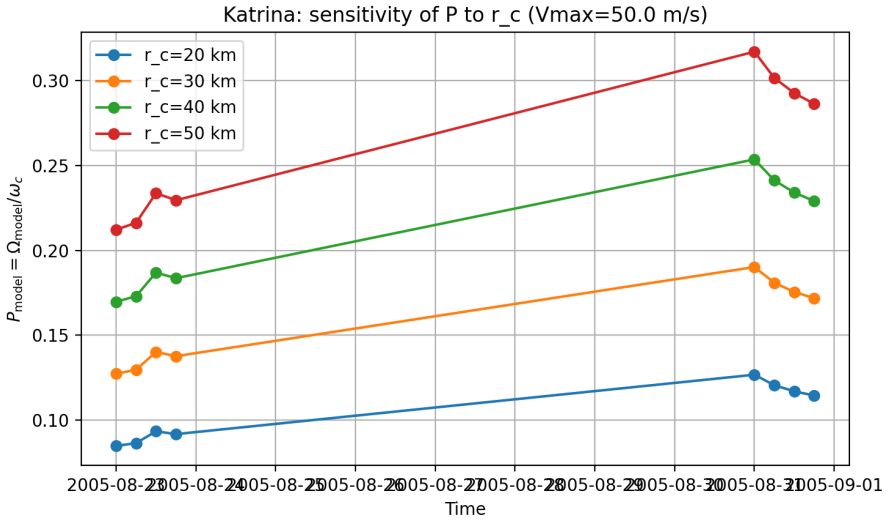


Figure 7. Sensitivity of the model-based precession number $P_{\mathrm{model}}(t)$ to the assumed inner-core radius r_c for the three analyzed storms. Across the full range $r_c \in [20, 50]$ km, the precession number remains below unity. For the smallest value ($r_c = 20$ km), peak values reach $P \sim 0.3$–0.4, while for $r_c \geq 30$ km the system operates within a clearly slow-precession regime ($P \lesssim 0.1$–0.2).

Although the strict asymptotic condition $P \ll 1$ becomes marginal for the smallest tested radius, the regime $P < 1$ is robust across the physically realistic interval. For typical inner-core values (30–50 km), the ordering $\Omega_p \ll \omega_c$ is well satisfied, supporting the slow-precession assumption adopted in the reduced-order framework.

5.6. Order-of-Magnitude Comparison Between Observed and Modelled Centre Wandering

Although the reduced model is not intended as a storm-specific hindcast, it is instructive to compare the characteristic amplitude of observed centre wandering with the corresponding precession scale used in the model. From the tracker-only decomposition of best-track positions (Figures 3–5), we define a characteristic wobble amplitude

$$A_{\mathrm{obs}} = \sqrt{\langle |\boldsymbol{r}'(t)|^2 \rangle}, \tag{15}$$

where $\boldsymbol{r}'(t)$ denotes the residual centre displacement relative to the smoothed guiding track.

For the three cyclones considered, A_{obs} typically lies in the range 10–30 km, with episodic larger excursions. In the reduced precessing-vortex model, the corresponding geometric scale controlling lateral wandering is the precession radius R_p. In the cyclone-like configuration, R_p is chosen in the range 50–100 km, leading to modelled lateral displacements that are consistent in order of magnitude with the observed wobble amplitude. We additionally report control experiments using $R_p = \mathrm{median}(A_{\mathrm{obs}})$ to provide a transparent comparison with the tracker-derived wobble amplitude, alongside larger illustrative values.

This comparison is not meant as a quantitative validation, but as an order-of-magnitude consistency check: both the observational analysis and the reduced model operate in a regime where centre wandering remains small compared to the storm-scale translation, yet large enough to produce significant cumulative lateral displacement over multi-day time scales. The agreement at the level of characteristic amplitudes supports the interpretation of R_p as a physically reasonable proxy for track-scale vortex wandering.

6. Discussion

The present framework deliberately operates at a reduced level of dynamical complexity. Rather than attempting to reproduce the full three-dimensional structure of tropical cyclones, it isolates a single mechanism slow shear-driven gyroscopic precession and investigates its transport-scale implications.

6.1. What the Tracker-Derived Wobble Constrains

The tracker-only decomposition isolates a residual displacement of the reported storm centre around a smoothed guiding track. Because best-track products are designed to provide a consistent estimate of the large-scale storm position, the extracted residual should be interpreted as a *track-scale wandering mode*, rather than as a direct measurement of inner-eyewall oscillations, mesovortices, or other sub-hourly inner-core dynamics. Accordingly, the diagnostics derived here constrain the low-frequency component of centre motion, with dominant time scales of order 1–3 days, consistent with classical descriptions of trochoidal motion in tropical cyclones.

Figures 3–5 illustrate this decomposition for three contrasting storms. In each case, the observed centre trajectory exhibits a slow wobble superimposed on a smoother guiding motion. A minimal kinematic reconstruction obtained by adding a constant precession to the guiding track reproduces the amplitude and characteristic scale of the observed wandering, indicating that a simple precessional description is sufficient to capture the dominant track-scale modulation.

6.2. Order-of-Magnitude Regime Selection via the Precession Number

A key result emerging consistently from all three cases is the smallness of the inferred non-dimensional precession number $P_{\mathrm{obs}} = \Omega_{\mathrm{obs}}/\omega_c$. As shown in the lower panels of Figures 3–5, $|P_{\mathrm{obs}}|$ typically remains $\mathcal{O}(10^{-2})$, with intermittent spikes associated with small residual amplitudes and phase ill-conditioning. This provides a data-based justification for the asymptotic ordering assumed in the reduced model, namely a fast internal vortex rotation combined with a slow gyroscopic degree of freedom ($P \ll 1$).

Differences among the three storms are physically interpretable within the definition of P_{obs}. Hyacinthe exhibits a slightly larger mean $|P_{\mathrm{obs}}|$ primarily because its inferred internal angular velocity $\omega_c \sim V_{\max}/r_c$ is smaller, so a comparable track-scale precession rate Ω_{obs} yields a larger non-dimensional ratio. Katrina and Hugo, by contrast, display similar values of ω_c and $\langle|\Omega_{\mathrm{obs}}|\rangle$, leading to comparable but slightly smaller $|P_{\mathrm{obs}}|$. This sensitivity highlights a practical limitation of track-only diagnostics: when only $V_{\max}$ is available, the inferred precession number depends linearly on the assumed inner-core length scale r_c. Replacing r_c by an estimate of the radius of maximum wind, when available, or propagating uncertainty bands over a plausible range (e.g., $r_c = 20$–50 km) is therefore recommended.

6.3. Precession as a Reduced-Order Proxy for Asymmetric Dynamics

Trochoidal motion and low-frequency centre meander have been linked to a variety of asymmetric mechanisms, including wavenumber-one disturbances, vortex Rossby waves, and boundary-layer interactions. The present analysis does not attempt to diagnose these processes from inner-core fields. Instead, it extracts an *effective* precession rate that summarizes their net impact on the slow lateral motion of the vortex centre at the track scale.

Observed trochoidal motion in tropical cyclones is often associated with azimuthal wavenumber-one ($m = 1$) asymmetries and vortex Rossby wave activity in the inner core. Such disturbances can displace the vorticity centroid relative to the guiding centre and may induce a slow rotation of this displacement vector about the storm centre. At track scale, the resulting motion can therefore appear as a slow precession of the apparent vortex position.

The present reduced-order formulation does not explicitly resolve $m = 1$ wave dynamics. Instead, it introduces a slow precession degree of freedom that acts as a kinematic coarse-grained representation of centroid displacements produced by unresolved asymmetric processes. In this interpretation, the precession variable encodes the macroscopic effect of inner-core asymmetries, while the instantaneous velocity field remains axisymmetric. This modelling choice reflects a deliberate scale separation: fast inner-core dynamics are not resolved, whereas slow centroid drift under weak environmental forcing is retained. The framework should therefore be viewed as complementary to fully non-axisymmetric simulations rather than as a replacement for them. From this perspective, the precession variable should not be interpreted as a substitute for resolving non-axisymmetric dynamics, but as a coarse-grained projection of their low-frequency centroid effect. This projection makes explicit a scaling relation that remains implicit within fully resolved simulations.

From a fluid-mechanics perspective, the value of introducing an explicit precession variable lies in its ability to represent slow wandering superimposed on fast swirl within a compact, analytically tractable framework. In this sense, $\Omega_p(t)$ should be viewed as a coarse-grained proxy that captures the cumulative effect of complex asymmetric dynamics, rather than as a claim about a unique underlying physical instability. The tracker-derived precession number therefore acts as a *model-regime selector*, identifying a realistic parameter range in which a reduced precessing-vortex description is appropriate.

6.4. Why Small Precession Numbers Still Matter

Although the inferred precession numbers are small, their dynamical impact accumulates over long vortex lifetimes. As illustrated by the multi-day wandering visible in Figures 3–5, even weak precession produces lateral displacements that are negligible on short time scales but become significant when integrated over days. This scaling explains how modest values of P can lead to kilometre-scale excursions in tornado-like regimes and $\mathcal{O}(10^2)$ km deviations in cyclone-like regimes.

Across scales, precession primarily acts as a *Lagrangian mixer*. By shifting the vortex core relative to its surroundings, it enlarges the effective footprint of air parcels that would otherwise remain confined near a steadily rotating core, thereby enhancing lateral transport and exchange with the environment. This effect is not readily captured by axisymmetric reduced models without an explicit wandering degree of freedom.

6.5. Limitations and Scope

The present framework is intentionally minimal. It is barotropic and vertically reduced, with vertical structure encoded only through a prescribed stretching rate and convective depth. Environmental couplings linking CAPE, shear, and background vorticity to $(a^\star, \Gamma^\star, \Omega_p^\star)$ are phenomenological and not statistically calibrated. Furthermore, the implementation assumes a circular precession orbit of fixed radius, whereas real wandering can be intermittent, non-circular, and multi-scale.

These limitations delimit the intended scope of the model. The analysis presented here is not a storm-specific hindcast, nor a validation of any particular physical mechanism. Rather, it provides an order-of-magnitude, regime-consistent demonstration that slow precession is a plausible and dynamically relevant ingredient for reduced-order descriptions of atmospheric vortex wandering. In this sense, the precession rate Ω_p should be interpreted as an effective, coarse-grained descriptor of low-frequency asymmetry rather than a direct diagnostic of a specific dynamical instability.

Relation to Comprehensive Dynamical Models and Analytical Insight

Operational dynamical models resolve a broad spectrum of interacting processes relevant to tropical cyclone evolution, including convection, microphysics, boundary-layer fluxes, and environmental flow coupling. While such models are indispensable for prediction, the large number of coupled degrees of freedom often makes it difficult to isolate specific mechanistic pathways. In particular, the relative role of weak environmental shear in generating slow centroid drift can remain embedded within nonlinear interactions between asymmetric convection, inner-core dynamics, and large-scale forcing.

By contrast, the present reduced-order formulation deliberately suppresses fast internal degrees of freedom and introduces gyroscopic precession as an explicit dynamical variable. This analytical transparency allows the dimensionless precession number $P = \Omega_p/\omega_c$ to emerge as a structural control parameter governing the ordering between intrinsic vortex rotation and slow centre displacement. In doing so, the framework reveals scaling relationships and asymptotic regimes that may remain implicit in fully coupled simulations.

The goal of the model is therefore not to replace comprehensive numerical approaches, but to provide mechanistic interpretability: by collapsing the dynamics onto a small set of physically interpretable parameters, it clarifies how weak environmental shear can produce order-one modifications of long-time Lagrangian transport through slow precessional motion.

6.6. Outlook

Future work may focus on calibrating the reduced parameters against high-resolution numerical simulations, introducing minimal dynamics for asymmetric (e.g., wavenumber-one) modes, and quantifying transport using objective mixing diagnostics. Within this perspective, the reduced precessing-vortex model provides a compact analytical bridge between large-scale environmental variability and vortex-scale transport across a wide range of atmospheric regimes [27,28].

In summary, the reduced-order approach adopted here sacrifices structural detail in exchange for analytical clarity. Its value lies in exposing a scaling-controlled regime—characterized by $P < 1$—in which weak environmental shear can nonetheless induce order-one modifications of long-time Lagrangian transport. Such structural insight complements comprehensive numerical models and may guide interpretation of their results.

7. Conclusions

This study introduced a reduced-order framework designed to represent slow lateral wandering of intense atmospheric vortices within an analytically tractable setting. Motivated by the widespread observation of trochoidal-like centre motion and the absence of precession in most reduced-order models, the approach treats gyroscopic precession as an explicit, weakly coupled degree of freedom superimposed on a rapidly rotating vortex core.

The vortex is modelled using a Burgers–Rott-type velocity field with slowly varying stretching rate and circulation, while the centre position evolves according to a precession kinematics governed by a rate $\Omega_p(t)$. Environmental variability enters the model through simple relaxation closures driven by standard diagnostics such as convective available potential energy, vertical shear, and background vorticity.

A tracker-only analysis of tropical cyclone best-track data shows that observed centre wandering typically operates in a regime where the precession number $P = \Omega_p/\omega_c$ is small, providing an empirical constraint consistent with the asymptotic structure of the model. Within this regime, numerical experiments demonstrate that weak precession can nonetheless accumulate over time to produce substantial lateral displacement and enhanced Lagrangian transport in cyclone-like configurations.

The present framework is not intended as a predictive storm model, but as a proof-of-concept reduced description that isolates the dynamical consequences of slow precession in rotating vortices. By clarifying how weak, environmentally forced wandering can shape vortex-scale transport, it provides a compact fluid-mechanical bridge between idealized vortex dynamics and large-scale environmental variability, and a natural starting point for future calibration and validation studies. As such, it complements detailed numerical and observational studies by providing a tractable reduced-order laboratory for exploring the cumulative effects of weak asymmetries on vortex-scale transport.

Funding: This research received no external funding.

Institutional Review Board Statement: Not applicable.

Informed Consent Statement: Not applicable.

Data Availability Statement: The data presented in this study are available on request from the corresponding author.

Conflicts of Interest: The authors declare no conflicts of interest.

Appendix A. Data-Driven Precession Extraction and Minimal Model Implementation

This appendix provides the full algorithmic workflow used to extract an effective precession signal from observed cyclone tracks and to construct the minimal precessing-track model discussed in Section 4. All steps are deterministic and reproducible, and the procedure can be implemented directly in any high-level language (e.g., Python 3.10 or MATLAB). The workflow isolates the low-frequency trochoidal component of storm-centre motion, estimates an effective precession rate and number, and reconstructs an idealized precessing-core trajectory for comparison with observations. An optional extension links the precession rate to environmental shear diagnostics derived from ERA5.

Appendix A.1. Case Selection and Analysis Window

Representative tropical cyclones are selected from best-track datasets (e.g., HURDAT2 or IBTrACS). For each storm, a time window is defined to encompass the mature-intensity phase—from the first hurricane classification (Category 1) to the onset of weakening. Only the storm-centre position and, when available, the maximum sustained wind $V_{\max}(t)$ are used; no wind-field or intensity model is required.

Appendix A.2. Tracker Data and Temporal Regridding

Best-track positions are provided at 6 h intervals. To facilitate differentiation and spectral analysis, the time series $(\mathrm{lat}(t_i), \mathrm{lon}(t_i))$ are interpolated onto a regular grid

$$t_n = t_0 + n\,\Delta t, \qquad n = 0, \ldots, N, \tag{A1}$$

with Δt chosen between 1 and 3 h depending on the case. Linear interpolation is sufficient, although cubic splines may be used for smoothness. When available, $V_{\max}(t)$ is interpolated to the same grid.

Appendix A.3. Conversion to Local Planar Coordinates

To express positions in consistent length units, the interpolated track is projected onto a local tangent plane centred on the mean location of the analysis window:

$$\mathrm{lat}_0 = \frac{1}{N+1}\sum_{n=0}^{N}\mathrm{lat}(t_n), \qquad \mathrm{lon}_0 = \frac{1}{N+1}\sum_{n=0}^{N}\mathrm{lon}(t_n), \tag{A2}$$

and

$$X(t_n) = R_E\cos(\mathrm{lat}_0)\big(\mathrm{lon}(t_n) - \mathrm{lon}_0\big), \tag{A3}$$

$$Y(t_n) = R_E\big(\mathrm{lat}(t_n) - \mathrm{lat}_0\big), \tag{A4}$$

where lat and lon are expressed in radians and $R_E = 6371$ km is the Earth's radius. This yields planar coordinates $\mathbf{r}_{\mathrm{obs}}(t_n) = (X(t_n), Y(t_n))$ in kilometres.

Appendix A.4. Track Decomposition into Slow Steering and Residual Wobble

The observed track is decomposed into a slowly varying "guiding-centre" component $\mathbf{r}_s(t)$ and a residual $\mathbf{r}'(t)$:

$$\mathbf{r}_{\mathrm{obs}}(t) = \mathbf{r}_s(t) + \mathbf{r}'(t), \qquad \mathbf{r}'(t) = \mathbf{r}_{\mathrm{obs}}(t) - \mathbf{r}_s(t). \tag{A5}$$

The slow component is obtained by temporal smoothing of (X, Y) with a window length T_s:

$$X_s(t_n) = \frac{1}{K}\sum_{|m-n|\le K/2} X(t_m), \qquad Y_s(t_n) = \frac{1}{K}\sum_{|m-n|\le K/2} Y(t_m), \tag{A6}$$

where K is an odd integer such that $K\,\Delta t \simeq T_s$. Typical values are $T_s = 24$–36 h, which retain the large-scale steering motion while filtering the subdaily residual wobble. Sensitivity tests with $T_s \in \{24, 36, 48\}$ h confirm that derived quantities are robust to moderate variations of this choice.

The residual amplitude and phase are defined as

$$A_{\mathrm{obs}}(t_n) = \sqrt{X'(t_n)^2 + Y'(t_n)^2}, \tag{A7}$$

$$\phi_{\mathrm{obs}}(t_n) = \mathrm{atan2}\big(Y'(t_n), X'(t_n)\big), \tag{A8}$$

with ϕ_{obs} unwrapped to remove 2π discontinuities.

Appendix A.5. Effective Precession Rate and Characteristic Period

An instantaneous angular rate is obtained by centred differencing of the unwrapped phase:

$$\Omega_{\mathrm{obs}}(t_n) \simeq \frac{\phi_{\mathrm{obs}}(t_{n+1}) - \phi_{\mathrm{obs}}(t_{n-1})}{2\,\Delta t}, \tag{A9}$$

where Δt is expressed in seconds. The dominant precession period is estimated either from the mean absolute rate $T_p \simeq 2\pi/\langle|\Omega_{\mathrm{obs}}|\rangle$, or from the peak frequency ω_{peak} of the power spectrum of the complex residual signal $z(t_n) = X'(t_n) + iY'(t_n)$, for which $T_p = 2\pi/\omega_{\mathrm{peak}}$. Both estimates generally agree within 10–20%.

Appendix A.6. Internal Angular Velocity and Dimensionless Precession Number

A characteristic internal angular velocity is defined from the best-track wind data as

$$\omega_c = \frac{\overline{V_{\max}}}{r_c}, \tag{A10}$$

where $\overline{V_{\max}}$ is the mean maximum sustained wind over the analysis window and r_c a representative core radius (e.g., 30 km for tropical cyclones, 300 m for tornadoes). The observed dimensionless precession number is then

$$P_{\mathrm{obs}}(t_n) = \frac{\Omega_{\mathrm{obs}}(t_n)}{\omega_c}. \tag{A11}$$

Typical values $P_{\mathrm{obs}} \sim 10^{-3}$–$10^{-2}$ indicate precession that is much slower than internal rotation.

Appendix A.7. Minimal Precessing-Track Model

To reproduce the observed wobble kinematically, we construct a reduced precessing-core trajectory

$$\mathbf{r}_{\mathrm{mod}}(t) = \mathbf{r}_s(t) + R_p(\cos\phi(t), \sin\phi(t)), \qquad \dot{\phi}(t) = \Omega_p(t), \tag{A12}$$

with R_p and Ω_p inferred from observations or environmental forcing.

Variant A—Tracker-only proof of concept.

For the minimal case, Ω_p is set constant from the dominant observed period, $\Omega_p = 2\pi/T_p$, and the precession radius is chosen as $R_p = \mathrm{median}(A_{\mathrm{obs}})$ or $R_p = \sqrt{\langle A_{\mathrm{obs}}^2 \rangle}$. The phase is integrated explicitly on the same temporal grid, $\phi(t_{n+1}) = \phi(t_n) + \Omega_p\,\Delta t$, with $\phi(t_0) = \phi_{\mathrm{obs}}(t_0)$.

Variant B—Optional ERA5-driven extension.

To introduce environmental coupling, the precession rate can be driven by a relaxation law:

$$\frac{\mathrm{d}\Omega_p}{\mathrm{d}t} = \frac{\Omega_p^\star(t) - \Omega_p(t)}{\tau_\Omega}, \qquad \Omega_p^\star(t) = \alpha\,|S(t)|, \tag{A13}$$

where $S(t)$ is a bulk vertical shear diagnostic from ERA5, α a gyroscopic proportionality factor, and τ_Ω an adjustment time scale (typically 6–24 h). Here we first compute the standard 200–850 hPa bulk shear magnitude $S_{\mathrm{trad}}(t) = \sqrt{(u_{200} - u_{850})^2 + (v_{200} - v_{850})^2}$ (in $\mathrm{m\,s^{-1}}$), and then define an effective shear rate $|S(t)| = S_{\mathrm{trad}}(t)/\Delta z$ with $\Delta z \approx 12$ km representing the vertical separation between the 850 and 200 hPa levels.

Integration of this equation followed by $\dot{\phi} = \Omega_p$ yields a time-varying precession consistent with environmental fluctuations.

Appendix A.8. Comparison Metrics

Observed and modelled residuals are compared using:

1. *Amplitude statistics:* mean, median, and RMS of A_{obs} and A_{mod}.
2. *Temporal scales:* dominant spectral period and bandwidth of the complex residuals $z(t)$ and $z_{\mathrm{mod}}(t)$.
3. *Dimensionless parameters:* comparison of $P_{\mathrm{obs}}(t)$ and $P_{\mathrm{mod}}(t) = \Omega_p(t)/\omega_c$.

Agreement is interpreted at the level of order of magnitude, consistent with the proof-of-concept scope.

Appendix A.9. Optional Lagrangian Tracer Demonstration

To visualize the kinematic impact of precession on mixing, passive tracers are advected in a Burgers-type vortex whose centre follows either the guiding centre $\mathbf{r}_s(t)$ (no precession) or the precessing trajectory $\mathbf{r}_{\mathrm{mod}}(t)$. Tracer dispersion and deformation of the near-core cloud are compared between the two cases, highlighting how even weak precession ($P \ll 1$) can enhance lateral spreading and effective mixing.

Appendix A.10. Implementation Summary

The full workflow consists of:

1. Loading and interpolating best-track data $(t, \mathrm{lat}, \mathrm{lon}, V_{\max})$.
2. Projecting to planar coordinates (X, Y).
3. Computing the smoothed track (X_s, Y_s) and residuals (X', Y').
4. Deriving A_{obs}, ϕ_{obs}, Ω_{obs}, T_p, ω_c, and P_{obs}.
5. Building the modelled trajectory $\mathbf{r}_{\mathrm{mod}}(t)$ (Variant A or B) and associated diagnostics.
6. Generating figures comparing tracks, residual spectra, and precession statistics.

This deterministic pipeline ensures full reproducibility and a transparent link between observational data and model variables.

Appendix B. Data Source and Dimensionality

The environmental forcing used in this study is derived from the ERA5 reanalysis produced by the European Centre for Medium-Range Weather Forecasts (ECMWF) [29]. ERA5 provides gridded atmospheric fields on a regular latitude–longitude grid and a set of vertical pressure levels. In the present work, we make use of:

- Two-dimensional horizontal fields (surface wind components, surface thermodynamic variables) at the model grid, and
- Vertical profiles of temperature, humidity and wind, from which column-integrated diagnostics such as CAPE and bulk vertical shear are computed.

For the cyclone-like case study, these two-dimensional horizontal fields and vertical profiles are sampled at a single grid point in a major-hurricane environment over the Gulf of Mexico during the life cycle of Hurricane Katrina. The resulting time series of $\mathrm{CAPE}(t)$, bulk shear $S(t)$ and large-scale vorticity $\zeta_{\mathrm{env}}(t)$ are used as realistic, but non-calibrated, large-scale forcings for the reduced precessing-vortex model. This case is intended as a proof of concept for ERA5-driven forcing, rather than as a detailed hindcast of Katrina.

References

1. Bluestein, H.B. *Synoptic–Dynamic Meteorology in Midlatitudes, Vol. II: Observations and Theory of Weather Systems*; Oxford University Press: New York, NY, USA, 1993.
2. Bluestein, H.B. *Severe Convective Storms and Tornadoes: Observations and Dynamics*; Springer: Dordrecht, The Netherlands, 2013.
3. Markowski, P.; Richardson, Y. *Mesoscale Meteorology in Midlatitudes*; John Wiley & Sons: Chichester, UK, 2010.
4. Burgers, J.M. A mathematical model illustrating the theory of turbulence. *Adv. Appl. Mech.* **1948**, *1*, 171–199.
5. Rott, N. On the viscous core of a line vortex. *Z. Für Angew. Math. Und Phys.* **1958**, *9*, 543–553. [CrossRef]
6. Davies-Jones, R. Tornado dynamics. *Atmos. Res.* **2006**, *83*, 389–401.
7. Sullivan, R.D. A two-cell vortex solution of the Navier–Stokes equations. *J. Aerosp. Sci.* **1959**, *26*, 767–768.
8. Kambe, T. Stabilization of columnar vortices. *J. Phys. Soc. Jpn.* **1986**, *55*, 4149–4156.
9. Kim, S.; Bryan, G.R. Development and evolution of tornado-scale vortices in a simulated supercell storm. *J. Atmos. Sci.* **2017**, *74*, 3993–4018.
10. Elsaesser, G.S.; Bryan, G.R. Effects of surface drag on tornado evolution and intensity. *J. Atmos. Sci.* **2018**, *75*, 2979–2997.
11. Lewellen, D.C.; Lewellen, W.S. Near-surface intensification of tornado vortices. *J. Atmos. Sci.* **2007**, *64*, 2176–2194. [CrossRef]
12. Willoughby, H.E. Linear motion of tropical cyclones. *J. Atmos. Sci.* **1992**, *49*, 289–303.
13. Holland, G.J. The maximum potential intensity of tropical cyclones. *J. Atmos. Sci.* **1997**, *54*, 2519–2541. [CrossRef]

14. Wurman, J.; Gill, J. Finescale radar observations of tornadoes. *Mon. Weather Rev.* **1997**, *125*, 213–230.
15. Orf, L.; Whiton, R.S.; Dahl, J.M.; Bluestein, H.B. Evolution of tornado vortices within a simulated supercell storm. *J. Atmos. Sci.* **2017**, *74*, 3441–3463.
16. Montgomery, M.T.; Kallenbach, R.J. A theory for vortex Rossby waves and its application to spiral bands and intensity changes in hurricanes. *Q. J. R. Meteorol. Soc.* **1997**, *123*, 435–465. [CrossRef]
17. Reasor, P.D.; Montgomery, M.T.; Bosart, L.F. Mesoscale observations of the genesis of Hurricane Felix (1995). *Mon. Weather Rev.* **2000**, *128*, 2716–2734.
18. Billant, P.; Chomaz, J.-M. Experimental evidence for a global mode in swirling jets. *J. Fluid Mech.* **1998**, *376*, 183–219. [CrossRef]
19. Derksen, J.J. Simulation of vortex breakdown and confined swirling flows. *Comput. Fluids* **2005**, *34*, 301–318. [CrossRef]
20. Syred, N. A review of oscillation mechanisms and the role of the precessing vortex core (PVC) in swirl combustion systems. *Prog. Energy Combust. Sci.* **2006**, *32*, 93–161. [CrossRef]
21. Manoharan, S.; Sharma, A.S.; Lieuwen, J.M. Precessing vortex core dynamics in swirling flows. *J. Fluid Mech.* **2020**, *903*, A16.
22. Mouhali, W.; Lehner, T.; Léorat, J.; Vitry, R. Evidence for a cyclonic regime in a precessing cylindrical container. *Exp. Fluids* **2012**, *53*, 1693–1700. [CrossRef]
23. Herault, J.; Schneider, R.; Nore, C. Subcritical transition to turbulence of a precessing flow in a cylindrical vessel. *J. Fluid Mech.* **2015**, *771*, 182–219. [CrossRef]
24. Giesecke, A.; Stefani, F.; Stieglitz, R. Precession-driven flows and instabilities in rotating containers. *Annu. Rev. Fluid Mech.* **2024**, *56*, 293–322.
25. Bryan, G.H.; Rotunno, R. The Maximum Intensity of Tropical Cyclones in Axisymmetric Numerical Model Simulations. *Mon. Weather Rev.* **2009**, *137*, 1770–1789. [CrossRef]
26. Moffatt, H.K. *Magnetic Field Generation in Electrically Conducting Fluids*; Cambridge University Press: Cambridge, UK, 1978.
27. Truchelut, R.J.; Schreck, C.J. *The HURDAT2 Atlantic Hurricane Database: Updates and Corrections*; NOAA National Hurricane Center Technical Documentation: Miami, FL, USA.
28. Knapp, K.R.; Kruk, M.C.; Levinson, D.H.; Diamond, H.J.; Neumann, C.J. The International Best Track Archive for Climate Stewardship (IBTrACS). *Bull. Am. Meteorol. Soc.* **2010**, *91*, 363–376. [CrossRef]
29. Hersbach, H.; Bell, B.; Berrisford, P.; Hirahara, S.; Horányi, A.; Muñoz-Sabater, J.; Nicolas, J.; Peubey, C.; Radu, R.; Schepers, D.; et al. The ERA5 global reanalysis. *Q. J. R. Meteorol. Soc.* **2020**, *146*, 1999–2049. [CrossRef]

Disclaimer/Publisher's Note: The statements, opinions and data contained in all publications are solely those of the individual author(s) and contributor(s) and not of MDPI and/or the editor(s). MDPI and/or the editor(s) disclaim responsibility for any injury to people or property resulting from any ideas, methods, instructions or products referred to in the content.